

FLOW OVER A THREE-DIMENSIONAL TURRET

C.W. Hirt and R.P. Harper
Flow Science, Inc.
5/31/88

PURPOSE

There are many practical fluid dynamics problems involving flow over complicated structures. Obvious examples are airplanes and high performance cars and boats. In recent years there have been enormous strides made in the analysis of such flows using computational fluid dynamics. With the use of large computers and specific computational models designed to represent the fluid dynamic phenomena known to occur in these applications, it has been possible to compute highly accurate solutions. Nearly all analysis methods developed for aerodynamic applications have been directed toward streamlined aerodynamic shapes. On the other hand, relatively little work has been devoted to flows around bluff bodies.

In this technical note we present the results obtained with FLOW-3D for steady flow about a turret attached to the underside of a helicopter near its nose. Our goal is to demonstrate how FLOW-3D can be used to study this type of bluff body flow problem.

PROBLEM DESCRIPTION

Physical Description

A cross section of the helicopter nose and attached turret is shown in Fig. 1. The helicopter nose is assumed axisymmetric about a horizontal axis, while the turret is axisymmetric about a vertical axis. Relatively low speed air, 100 ft/s, is assumed to be flowing from left to right parallel to the axis of the helicopter.

The turret diameter is approximately 13.2 in, except for the truncated cone section, which is somewhat wider. The vertical extent of the turret below the helicopter body averages about 21.3 in. and its axis is located 21 in. aft of the leading edge.

The helicopter body consists of a spherical nose cap blended with an axisymmetric shape given by the equation

$$r = 1.608(22+x)^{0.71}, \quad (1)$$

with

$$r = (x^2+y^2)^{1/2},$$

where the coordinate origin is located at the intersection of the helicopter and turret symmetry axes. The turret is composed of cylindrical and spherical pieces with a truncated cone section in the middle.

Some Assumptions

To reduce the computational effort we will assume that the flow above the helicopter axis is symmetric with respect to that below so that a horizontal plane of symmetry can be defined at the axis. This is not correct, but the error this makes in the flow around the turret is not likely to be significant. Similarly, we shall assume there exists a vertical plane of symmetry through the helicopter's axis. Since the incident air flow is parallel to the axis this assumption is justified.

These symmetry assumptions rule out the possibility of modeling any unsteady flow that might be associated with vortex shedding from the turret assembly. Although vortex shedding is not very likely because the length to diameter of the turret is low (usually a ratio of 4 or 5 is necessary for vortex shedding), it is nevertheless important to recognize that this type of flow phenomena has been eliminated from our model.

Furthermore, for this demonstration problem all turbulence and viscous effects have been ignored. Our principal interest is in the flow and pressure distribution generated around the turret in steady flow conditions. By neglecting viscous effects we are overlooking possible details associated with the precise location of boundary layer separation points. Experience with other computations of the present type, using free slip boundary conditions, suggests that the results with respect to flow separation will approximate physical cases of relatively high turbulence levels. This situation arises because of the inherent smoothing associated with numerical approximations. In particular, there are some unavoidable smoothing errors in the momentum equations that introduce viscous-like effects.

Numerical Model

For our numerical model we shall use units of inches and seconds for length and time while mass will be measured in units of 12 slugs. The latter choice results in pressures expressed in psi.

The finite-difference mesh covers a region extending 44 in. below the helicopter axis, 30 in. to one side and 60 in. along the axis. The upstream boundary is 9 in. in front of the nose. A cell resolution of 20 by 10 by 16 mesh cells (or 4752 total cells including boundary cells) are in the mesh. In defining the mesh a couple of mesh line locations were specified to insure an optimal definition of the helicopter and turret geometries. For instance, one x location was set where the helicopter body and nose cap were joined. Also, several z locations were selected to match the boundaries where the component pieces of the turret were joined together. Figure 2 shows the mesh arrangement selected.

All obstacles in this problem, with the exception of the body of the helicopter, are easy to define using the standard FLOW-3D obstacle functions. To define the body, which involves a fractional exponent, we had to modify the basic function routine, FCNO(F1,F2,F3,KN). The most convenient way to do this is by redefining one of the terms not used by any of the other functions needed to specify the geometry. In the present case the coefficient, CRXY, of the radius r was a suitable choice. We modified the function routine as shown in continuation line 3 of the listing contained in Fig. 3. In order to use the coefficient of r this way we had to square the original equation (1), which converts r to $x^2 + y^2$ and doubles the exponent on the right side of Eq. 1 to 1.42. In this way we retain the same coordinate definition of the body but without using r as an independent variable so that CRXY can be used to multiply the modified function.

A complete input file defining the mesh specification, obstacle shape functions, physical and computational parameters and a selection of graphic outputs is given in Fig. 4. Selected plots showing the helicopter and turret geometry generated by the FLOW-3D preprocessor are contained in Fig. 5. Because of the coarseness of the mesh, the obstacle plotter was not able to define all details of the geometry. For example, it could not reproduce the spherical nose cap because it is contained within one computational mesh cell. It also missed some details around the turret and turret/helicopter intersection, which are on the order of one mesh cell. Even though the plotter is not able to show these details, this does not mean that the calculational model is incorrect. The difficulty is a plotting limitation

associated with the reconstruction of the geometry from the area/volume fractions of the mesh cells blocked by the obstacles.

Included in the input file are specifications for boundary conditions at all six boundaries of the mesh. Two of the boundaries are planes of symmetry. At the minimum x boundary a constant inflow velocity of 1200 in/s (100 ft/s) is prescribed in the positive x direction. Because we are treating the flow as incompressible, it isn't necessary to specify the temperature of the incoming fluid. Fluid density is constant at $1.21\text{E-}7$, corresponding to air at standard conditions in the present set of units (12 slugs/in^3). All remaining boundaries are defined as continuative, that is, as boundaries where the normal derivatives of all flow variables are zero.

Continuative boundaries are not true "physical" boundary conditions. Their use here reflects our expectation that the flow will be passing out through these surfaces and we want this to occur smoothly with a minimum effect on the upstream flow structure. As a general rule these boundaries should be placed as far away from the region of interest as possible. In the present case we have located them rather close to the turret in order to keep this demonstration problem to a modest size. It was for this same reason that we also placed the inflow boundary closer to the helicopter nose than is generally desirable.

The usual check on whether or not the inflow and outflow boundaries are sufficiently far removed is to repeat the calculations with the boundaries moved successively further away until no significant changes are detected in the flow region of interest. Performing this type of parameter study is particularly easy with FLOW-3D since it is only the mesh specification that needs to be modified in the input data file. All other input data (except some graphic requests) remain unchanged since they are specified in physical coordinates without reference to the mesh.

FLOW-3D is primarily a transient flow analysis code, however, in this example we are only interested in the steady flow limit. To accelerate convergence to steady conditions a useful technique that often works well is to limit the pressure iteration process, used to satisfy incompressibility, to one iteration per time cycle. This means that the computed transient flow is not accurate, but it reduces the cost of many passes (cycles) through the complete flow equations, which are needed to reach steady conditions. The input parameters used to set this acceleration procedure are a large pressure convergence criterion, $\text{EPSI}=1.0\text{E}+6$, and no overrelaxation, $\text{OMEGA}=1.0$. As we shall see, this technique needs to be used with some care in the present application.

COMPUTATIONAL RESULTS

While only steady state results are of interest, it is necessary to begin the calculations with some sort of initial condition and to then perform a time-like advancement until steady conditions are reached. In the present instance we set an initial velocity everywhere in the computational region equal to the specified inflow velocity of 1200 in/s. Because the flow is assumed incompressible, a uniform initial velocity does not satisfy the incompressibility condition of a zero divergence at obstacle surfaces. Fortunately, this does not matter for FLOW-3D automatically adjusts the velocities, through its pressure-velocity iteration procedure, to insure that they will satisfy the proper conditions. Restricting the pressure iteration to only one iteration per time step, however, means that the calculational results approximate a pseudo-compressible fluid that only satisfies the incompressibility condition when steady conditions are reached.

The calculation was run in several pieces because the time interval needed to reach a steady state was unknown. First, a problem time of 0.2 s was computed. This took 2.13 hr of CPU time on a MicroVAX II computer. Although the results looked quite good, close inspection showed that the velocity divergence was relatively large (of order 1) around the surface of the turret indicating that incompressible conditions had not been reached with sufficient accuracy. As a rule of thumb, the divergence should not be larger than about $2.0E-4$ times the ratio of a typical velocity divided by a mesh cell size. In this case, for example, the rule gives $2.0E-4(1200/2.2)$ or about 0.1 for the maximum divergence magnitude.

In an attempt to reduce the divergence we then restarted the calculation and ran it out to a problem time of 0.5 s. This took another 3.06 hr of CPU time. Unfortunately, the divergence was not significantly reduced. Previous experience suggested that the use of only one pressure iteration per time cycle was the culprit. Further analysis of the output data indicated that there were weak pressure oscillations which were not being damped. This has been observed in other calculations involving continuative outflow boundary conditions coupled with a weak convergence criterion for the pressure. The remedy is to reduce the convergence criterion and continue the calculation to steady conditions. In this case we set the desired convergence level to the 0.1 value and continued the calculation to a time of 0.6 s. A CPU time of 2.47 hr was needed for this continuation, but the results did converge quickly to the level of accuracy desired.

Hindsight indicates that the weak convergence criterion was useful for roughing out the basic flow structure, but that we should have switched to the tighter convergence level after the first run segment. By eliminating the middle segment it is probable that the calculation could have been successfully completed using only the first and last parts, i.e., with only 4.6 hr of CPU time.

Computed flow and pressure fields in the vertical symmetry plane are shown in Fig. 6. The mean flow is from left to right, however we can see that there is some reverse flow immediately behind the lower portion of the turret. As one might have expected there is a pressure minimum at the bottom of the turret. A pressure maximum (at least in this plane) occurs on the truncated cone portion of the turret. This is physically reasonable since the turret is more blunt than the helicopter nose and the cone segment is the widest part of the turret.

A significant pressure gradient exists around the leading edge of the truncated cone where there is a sharp turning of the flow around this edge. A somewhat weaker gradient is seen at the downstream edge of the cone.

It should be noted that some pressure variation exists along the lefthand inflow boundary, which indicates that a uniform inflow velocity is not quite consistent with the remaining flow. The only remedy for this would be to move the inflow boundary further to the left and repeat the calculation.

Figure 7 shows the computed velocities and pressures in two horizontal planes just above and just below the bottom surface of the cone segment in the turret. The horizontal extent of these plots has been limited to the immediate neighborhood of the turret in order to see the local details more clearly. In the plane cutting through the cone the pressure maximum is at the leading edge of the cone, while the pressure minimum is displaced slightly aft of the equator. This structure is reminiscent of flow over a cylinder.

On the cylindrical section immediately below the cone, the pressure distribution is different. The maximum pressure is located slightly upstream of the leading edge of the cylinder and the minimum pressure is located upstream of the equator. Thus, both extremes are shifted upstream with respect to the corresponding values on the cone section. We also note that the maximum pressure on the cylindrical section is only about half the maximum value on the cone section. This lower value and the shifts in extrema location reflect the turning of the flow over the sharp leading edge of the cone that was noted in Fig. 6.

The pressure variation around the cylinder under the cone is about 0.088 psi, which is approximately equal to the dynamic head of the incoming flow, $\rho u^2/2 = 0.087$ psi.

There is a recirculation region behind the cylinder, Fig. 7, which results in a fairly uniform pressure over the rear surface of the cylinder. No corresponding recirculation is seen behind the cone section, probably because of the proximity of the helicopter body.

Figure 8 contains plots in three planes normal to the axis of the helicopter. One plane is located at the nose, one intersects the turret and the third is at the downstream end of the computational region. The flow vectors may appear a little strange because the principal velocity component is normal to these plots. Essentially the flow is being diverted out the sides of the computational mesh by the expanding body of the helicopter. Pressures also reflect this trend since the maximum pressure in each case is on the body, while the minimum pressure is at a mesh boundary.

SUMMARY

It has been stressed that the boundaries of the computing region should have been moved further away from the helicopter to reduce their influence on the flow around the turret. For this reason, the absolute pressures and velocities at the surface of the turret should be regarded with some caution. Nevertheless, the computed flow structure is quite interesting and appears realistic with respect to many details.

In addition to moving the boundaries further away, it would be worthwhile to increase the numerical resolution around the turret where detailed information is wanted. Also, any complete study should consider effects of viscous stresses, turbulence in the incident flow and possible variations in the incident flow profile. All of these effects can be investigated with FLOW-3D.

Although computational times are not really excessive for this three-dimensional problem, it is worth pointing out that the MicroVAX II is not a particularly fast computer. For instance, timing studies with FLOW-3D indicate that the new SUN 4/110 workstation computer, which is very reasonably priced, is at least four times faster. Thus, on the SUN the present results could be obtained in about 1 hr of CPU time.

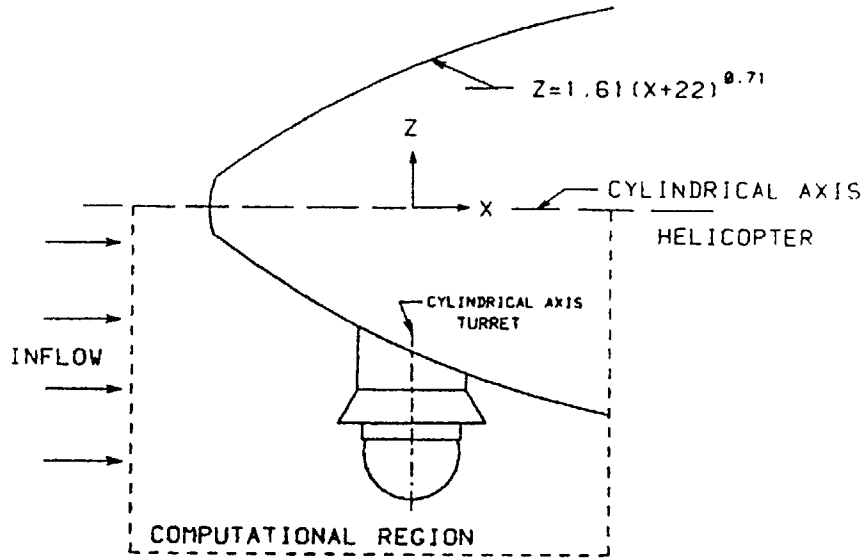


Fig. 1. Sketch of helicopter and turret arrangement showing regions modeled.

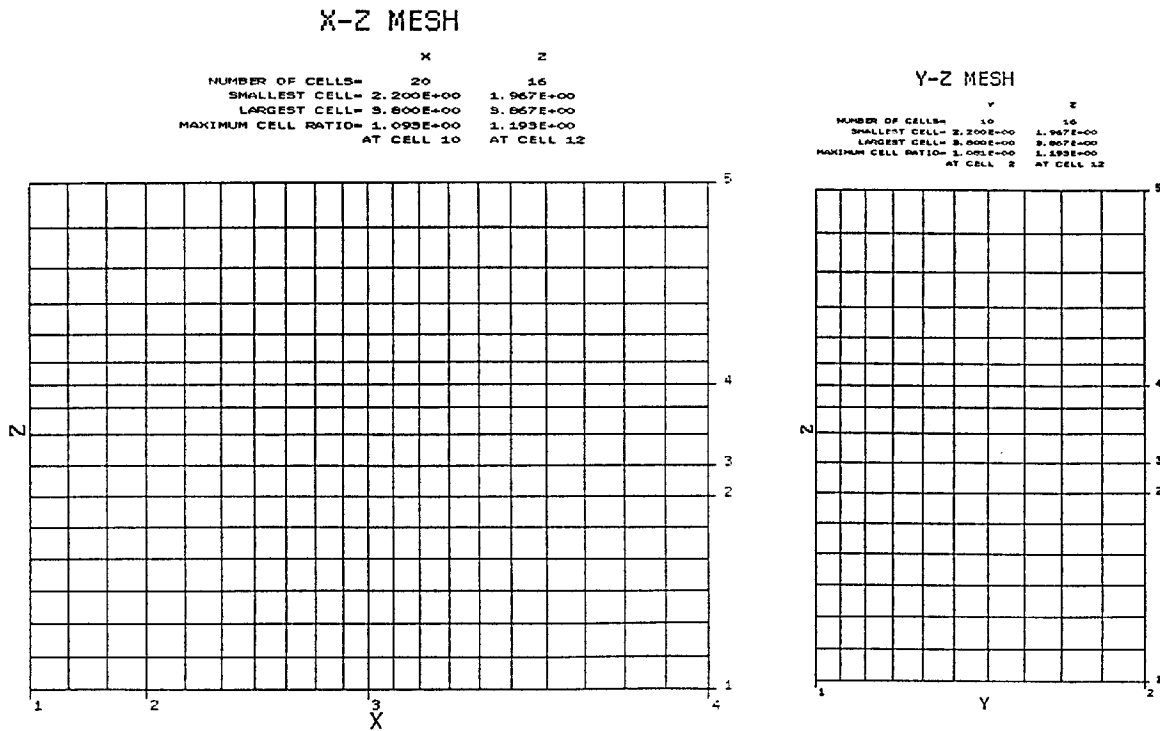


Fig. 2. Computational mesh.

```

FUNCTION FCN0(F1,F2,F3,KN)
C
C      ARBITRARY PARABOLIC FUNCTION EVALUATOR
C
C      INCLUDE 'COMDECK:PRECIS.FOR'
C      INCLUDE 'COMDECK:PARAMS.FOR'
C      INCLUDE 'COMDECK:OBS.D.FOR'
C      INCLUDE 'COMDECK:FUNC.FOR'
C
FCN0=CC(KN)+CX(KN)*F1+CY(KN)*F2+CZ(KN)*F3+
1      CXY(KN)*F1*F2+CXZ(KN)*F1*F3+CYZ(KN)*F2*F3+
2      CX2(KN)*F1*F1+CY2(KN)*F2*F2+CZ2(KN)*F3*F3+
3      CRXY(KN)*((FABS(F1+22.0))**1.42)-1.1E-10
RETURN
END

```

Fig. 3. Function routine used to define regions with change in continuation line 3 used to define helicopter body.

```

TURRET
$XPUT
      WL=6,          WR=3,          WBK=3,
      WB=3,          UBCT(1,1)=1200.,  UI=1200.,
      RHOF=1.21E-7, DELT=8.0E-4,  TWFIN=0.2,
      ILPR=8,        IRPR=16,       JBKPR=5,
      KBPR=8,        KTPR=12,       EPSI=1.0E+6,
      OMEGA=1.0,     AVRCK=-2.1,
$END
$MESH
      PX(1)=-30.,    PX(2)=-19.7,    PX(3)=0.0,
      PX(4)=30.,     SIZEX(3)=2.2,    NXCELT=20,
      PY(2)=30.,     SIZEY(1)=2.2,    NYCELT=10,
      PZ(1)=-44.,    PZ(2)=-27.2,    PZ(3)=-24.5,
      PZ(4)=-17.5,   PZ(5)=0.0,      SIZEZ(3)=2.7,
      NZCELL(3)=3,   NZCELT=16,
$END
$OBS
      NOBS=2,
      IOFO(1,1)=1,   CY2(1)=1.0,     CZ2(1)=1.0,
      CRXY(1)=-2.586, XL(1)=-19.7,    CX2(1)=1.0,    CY2(2)=1.0,
      IOFO(2,1)=2,   CX(2)=34.3,     CC(2)=279.3,
      CZ2(2)=1.0,    CX2(3)=1.0,     CY2(3)=1.0,
      XH(2)=-19.75,  ZL(3)=-17.5,    CX2(4)=1.0,    CY2(4)=1.0,
      IOFO(1,2)=3,   CX2(4)=1.0,     ZL(4)=-27.2,  CX2(5)=3.2217,  CY2(5)=3.2217,
      CC(3)=-46.24,  ZL(4)=-27.2,   CZ(5)=-10.5898,  CC(5)=-28.036,
      IOFO(2,2)=4,   CX2(5)=3.2217,  ZH(5)=-17.5,   CZ(6)=1.0,
      CC(4)=-43.56,  CZ(5)=-10.5898, ZH(5)=-17.5,   CZ(6)=1.0,
      IOFO(3,2)=5,   ZL(5)=-24.5,   CX2(6)=1.0,     CZ(6)=58.,     CC(6)=797.44,
      CZ2(5)=-1.0,  IOFO(4,2)=6,   CZ2(6)=1.0,
      ZL(5)=-24.5,  CZ2(6)=1.0,
      IOFO(4,2)=6,  CZ2(6)=1.0,
      CZ2(6)=1.0,  ZH(6)=-27.25,
      ZH(6)=-27.25,
$END
$FL
$END
$BF
$END
$TEMP
$END
$GRAFIC
      NCPLTS=3,      JC2(1)=2,        IC1(2)=6,
      IC2(2)=18,     JC2(2)=8,        KC1(2)=8,
      KC2(2)=8,      IC1(3)=6,        IC2(3)=18,
      JC2(3)=8,      KC1(3)=9,        KC2(3)=9,
      NVPLTS=4,      JV2(1)=2,        IV1(2)=6,
      IV2(2)=18,     JV2(2)=8,        KV1(2)=8,
      KV2(2)=8,      IV1(3)=6,        IV2(3)=18,
      JV2(3)=8,      KV1(3)=9,        KV2(3)=9,
      IV1(4)=11,     IV2(4)=11,
      IOBSL=11,      IOBSR=11,        JOBSBK=2,
      KOBSD=8,       KOBST=9,
$END
$PARTS
$END

```

Fig. 4. Input file for turret problem.

